Egypt. J. Chem. **Vol. 64,** No. 8 pp. 4209 - 4231 (2021)

Egyptian Journal of Chemistry

http://ejchem.journals.ekb.eg/

Preparation of Titanium to Zirconium ZSM-5: Structure Elucidation and Photocatalytic Behaviour

Samia A. Kosa[*, 1], Islam H. Abd El Maksod [1, 2], Eman Z. Hegazy [1, 2] and Naha M. Al-sebaii[1]

[1]*Chemistry Department, Faculty of Science, King Abdulaziz University, Jeddah 21551, Saudi Arabia*

[2]*Physical Chemistry department, National Research Centre (NRC), Dokki, Cairo, Egypt*

Abstract

In this study, a series of Titanium to Zirconium ZSM-5 framework was prepared. Elucidations of the structure were performed using XRD, IR, DR, and SEM images. The results showed that Ti and/or Zr could exist in either tetrahedral or octahedral sites. Simultaneous dye photodegradation with the removal of heavy metal was performed and completely studied with four-dimensional curves. The analysis of the data showed that the metal ions could play an important role in the photodegradation mechanism of organic dye. Photodegradation mechanism is elucidated and kinetic studies showed that the degradation followed up pseudo-first-order kinetics. For the first time deconvolution of IR spectra could be assigned for the elucidation of the structure of prepared materials. The prepared materials are found to be efficient in multiple removals of organic/inorganic pollutants which raise its economic impact.

Keywords: ZSM-5, XRD, SEM, simultaneous removal, photodegradation, heavy metals.

1. Introduction

ZSM-5 (Zeolite Socony Mobil–5) zeolite structure attracted much attention for its unique pentacle pore channels system [1-3]. It was used as a catalyst for many reactions such as isomerization, alkylation of hydrocarbons [4-6]. Also, it could be used in the reduction of nitrogen oxide [7-10] due to its acidity on its surface. Loading transition metals on ZSM-5 such as iron is a traditional work for control its catalytic performance towards many catalytic reactions [11, 12]. Loading transition metals, however, only modify the surface structure but incorporation of foreign cation into the framework structure of ZSM-5 was utilized also to modify not only the surface but also the inner framework structure. Thus, incorporation of Ti into ZSM-5 was performed many years ago and the modified structure was abbreviated by TS-1 [13, 14]. TS-1 modified structure attracted many new applications such as its use as a photocatalyst [15, 16]. This may be due to the new materials containing Ti in its framework structure could generate a new photoactive site. In addition to Ti, Zr the second member of its group also seemed to have photocatalytic performance either in a separate oxide form or incorporated in other framework structures [17-20]. In this research, impeding of Ti, and Zr into ZSM-5 framework structure with different ratios was studied. The corresponding influence on the photocatalytic behavior and also the in exchange behavior towards ions and organic dye as a model system was also evaluated.

2. Experimental

2.1. Materials

All chemicals used for the preparation of ZSM-5 were analytical grade reagents as following:

Tetraethyl orthosilicate (TEOS) ($SiC_8H_{20}O_4$) (98%) (Merck), sodium hydroxide (NaOH) (Merck), titanium (IV) chloride ($TiCl_4$) (Merck), zirkonium (IV) Chloride ($ZrCl_4$) (Merck), tetrapropylammonium hydroxide (TPAOH), copper nitrate ($Cu(NO_3)_2.3H_2O$ (Sigma-Aldrich), nickel nitrate $Ni(NO_3)_2.6H_2O$ (Sigma-Aldrich), lead nitrate ($Pb(NO_3)_2$ (Sigma-

*Corresponding author e-mail: skousah@kau.edu.sa.; (Samia A Kosa).
Receive Date: 16 January 2021, Revise Date: 25 March 2021, Accept Date: 06 April 2021
DOI: 10.21608/EJCHEM.2021.58345.3256

Aldrich), cobalt nitrate ($Co(NO_3)_2.6H_2O$ (Sigma-Aldrich). methylene blue dye ($C_{16}H_{18}ClN_3S{\cdot}xH_2O$) (Sigma-Aldrich).

2.2. Preparation of ZSM-5

In a typical synthesis of Zr-ZSM-5, a solution of 9.4 g of TPAOH was added to 0.7 g of NaOH in 55 ml distilled water. Then, this solution (named solution A) was added slowly to solution B. Solution B was prepared by mixing 0.73 g of $ZrCl_4$ in 5 g of distilled water with 21.35 g of TEOS (0.933 g/mL) The whole mixture was stirred at 60-80°C for 1 hour. Then the mixture was left for 24 hours foraging and then autoclaved for 3 days at 175°C. After that, the mixture is washed filtered and dried. Titanium is introduced as a molar ratio replacing the Zirconium keeping the total number of moles of both constant shows in Table 1 to obtain five different ratios of Zr to Ti.

Table 1 Elemental comp (atomic ratio) in synthesizing mixture

sample	Si	Zr	Ti	Na	Si/Zr+Ti
100 % Zr	83.2	2.54	0	14.2	32.7
2Zr:1Ti	83.2	1.69	0.85	14.2	32.7
1Ti:1Zr	83.2	1.27	1.22	14.2	32.7
2Ti: 1Zr	83.2	0.85	1.69	14.2	32.7
100% Ti	83.2	0	2.54	14.2	32.7

2.3. Photocatalytic experiment

A 100mL of methylene blue was mixed with 0.1 g of the composite using a horizontal cylinder annular batch reactor. A mercury lamp (300 W) was used for irradiation of the photocatalyst. The photocatalytic reaction was carried out at room temperature. Different amounts of solutions are collected by time for analysis.

2.4. DRUV-VIS spectral data

DRUV–VIS (diffuse reflectance ultraviolet-visible) spectral data were collected using a Thermo-Scientific evolution spectrophotometer equipped with an integrating sphere in the wavelength range of 200–800 nm to measure the reflectance spectra of samples.

2.5. Inductively Coupled Plasma (ICP)

ICP analysis of metals was analyzed using Perkin Elmer Optima 7000 DV.

2.6. X-ray powder diffraction analysis (XRD)

X-ray powder diffraction (XRD) patterns were collected using the Rigaku X-ray diffractometer system equipped with a RINT 2000 wide-angle Goniometer using Cu Kα radiation (λ = 0.15478 nm) and a power of 40 kV×30 mA. Figure 2.1 shows the XRD device. The intensity data were collected at room temperature over a 2Θ ranging from 10 to 80°.

2.7. Scanning electron microscopy (SEM)

Samples were examined via a field emission scanning electron microscope (SEM) which was obtained using JEOL JSM-7600F. This system is combined with energy Dispersive X-ray spectroscopy for composition and elemental analysis.

2.8. Fourier-transform infrared spectroscopy (FTIR)

Perkin-Elmer Spectrum100 FTIR spectrometer was used to obtain FTIR spectra.

3. Results and discussion

3.1. XRD analysis

XRD diffraction patterns of all different ratios Zirconium to Titanium ZSM-5 phase are presented in Figure 1. All XRD patterns showed that only the ZSM-5 phase is obtained as the only phase compared to PDF Card No. P440002. Also, Figure 2 showed the relative crystallinity of all samples against % Ti. This curve showed that as % Ti increases the relative crystallinity decreased till reaches 50% after which a sudden increase in relative crystallinity to be 100% at 1Zr:2Ti after which it decreased again.

Crystal lattice analyses are presented in Table 2. From this table, it could be observed that all samples suffer from deviation from lattice parameters of corresponding Al ZSM-5. Also, the least deviation sample is the highest in relative crystallinity (1Zr:2Ti). Based on the angles and lattice constant we can give the sample order according to the degree of deviation (Table 2). Redraw the relative crystallinity again against this order (Figure 3). From this figure, it could be observed clearly that as the deviation increases the relative crystallinity decreases. This could be assigned to the ratio between Zirconium to Titanium. In other words, when this ratio approaches the value of being ideal to ZSM-5 crystal, the crystal growth is maximum which is being to be not directly correlated to values of the molar ratio of Zirconium to Titanium in the synthesizing mixture but to the real values entering the crystal of ZSM-5 which will be seen later from EDX analysis.

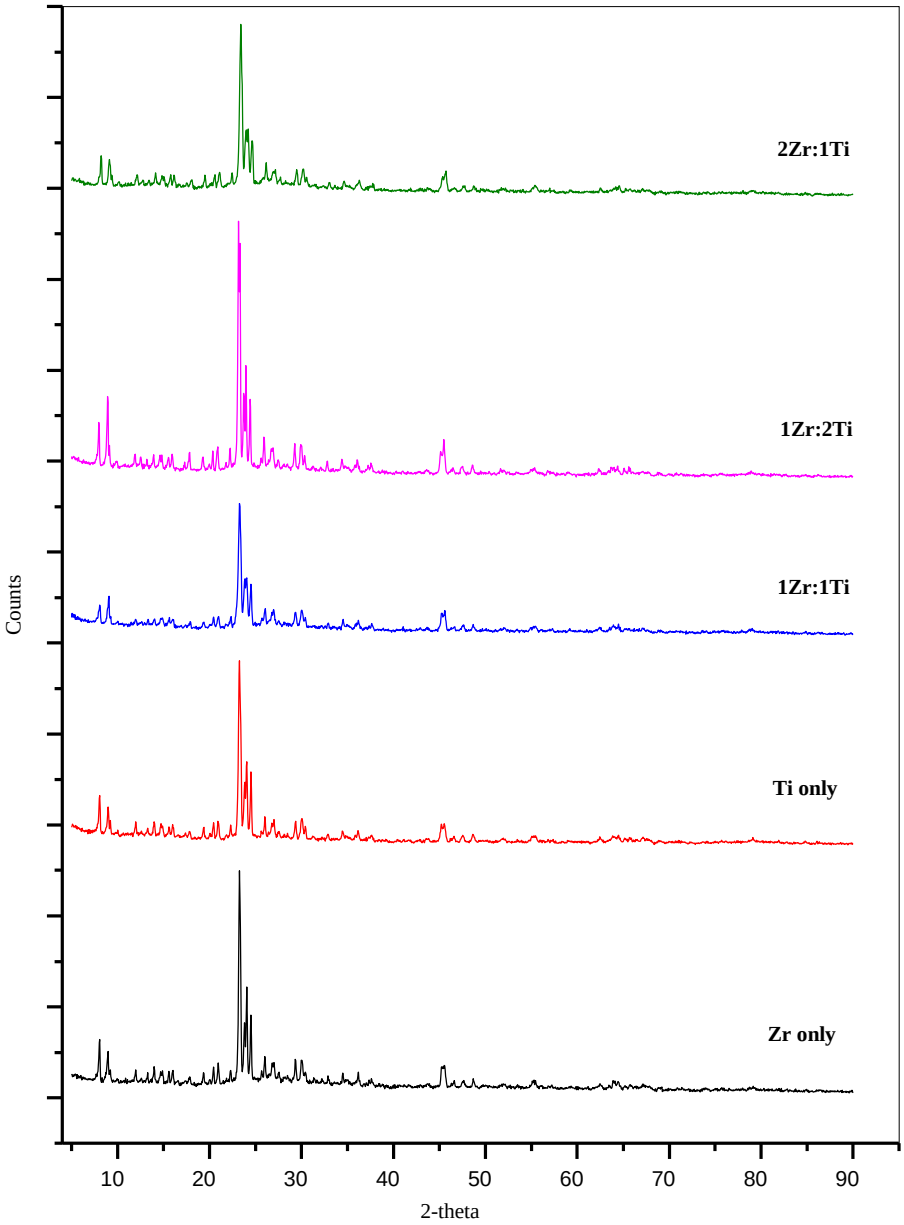

Figure 1 XRD patterns of all investigated samples

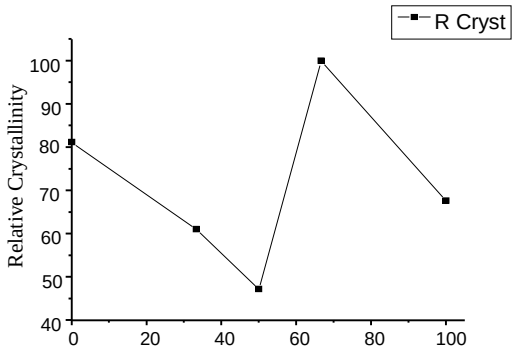

Figure 2 The relative crystallinity of all samples against % Ti.

Table 2 Crystal lattice analysis of all samples of part II

sample	Phase name	Crystal system	Deviation order from reference	a	b	c	α	β	ɤ
Reference PDF. P440002)	ZSM-5	Tetragonal		19.96	19.96	13.37	90	90	90
(Zr only)	ZSM-5	Orthorhombic	2	19.911	20	13.361	90	90	90
(Ti only)	ZSM-5	Monoclinic	3	29.685	20.665	7.794	90	95.079	90
(1Zr:1Ti)	ZSM-5	Monoclinic	5	41.75	18.773	12.152	90	92.863	90
(1Zr:2Ti)	ZSM-5	Orthorhombic	1	19.934	20.037	13.383	90	90	90
(2Zr:1Ti)	ZSM-5	Monoclinic	4	22.088	7.545	15.270	90	101.626	90

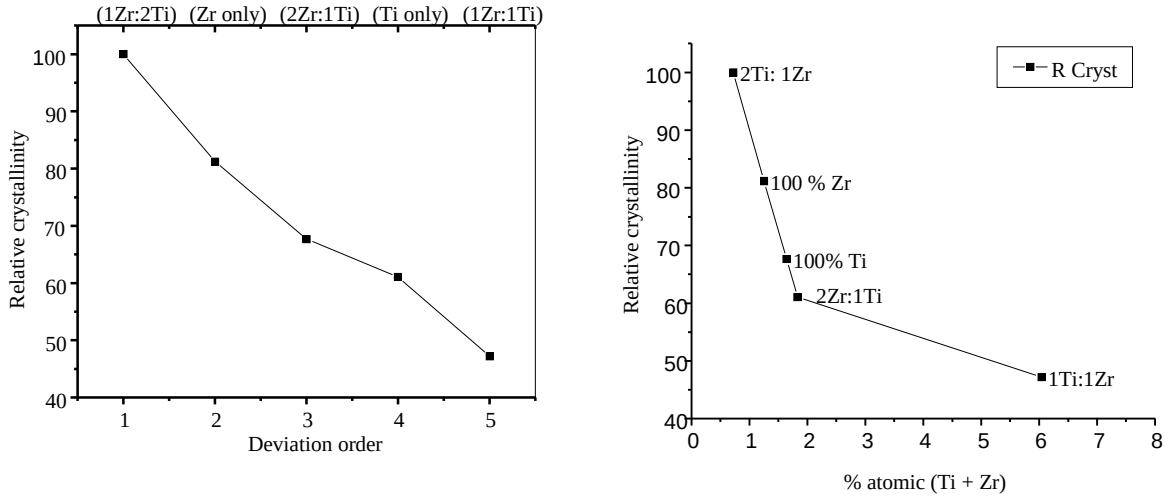

Figure 3 The relative crystallinity against deviation order and % of atomic (Ti+Zr)

3.2. SEM and EDX analysis

Figures (4) showed the SEM images of all samples studied with different ratios of Ti/Zr. These figures showed clearly the formation of ZSM-5 in well-formed crystals in all samples. However, an amorphous unshaped background appears also in all images. Also, spherical-shaped particles could be observed in mixed Zirconium to Titanium samples. These spherical-shaped particles may be precursors of the different or same type of crystals which is beyond the XRD detection limit. The EDX analysis of orthorhombic shaped crystals and also the spherical shaped ones are presented in Tables (3-4). From these Tables, it could be observed that Zr and Ti have existed in all crystals except that of the 2Zr:1Ti sample where only Zr is observed. This indicates that the incorporation of Ti and Zr in the crystal lattice of ZSM-5 crystals. The presence of Ti and Zr in all spherical-shaped and amorphous backgrounds indicates clearly that not all Zr and Ti in synthesizing mixture is included in the crystallization process of ZSM-5 crystals. The previous fact shed some light on the presence of Ti and Zr ions in different environments. Thus, they exist tetrahedrally in the ZSM-5 crystals and maybe tetrahedrally or octahedrally in amorphous and spherical-shaped particles.

Table 3EDX analysis of orthorhombic shapes

Sample	Si	O	Zr	Ti	Na	Si / (Ti+Zr)
100 % Zr	52.16	45.12	1.25		1.47	41.73
2Zr: 1Ti	29.43	67.95	1.83		1.69	16.08
1Ti: 1Zr	28.11	60.56	3.82	2.22	5.3	4.65
2Ti: 1Zr	23.85	74.11	0.72	0.43	0.89	20.73
100% Ti	29.05	69.19		1.64	0.975	17.71

Table 4 EDX analysis of spherical shapes in different samples

Sample	Si	O	Zr	Ti	Na	Si/(Zr+Ti)
1Ti:1Zr	19.69	70.64	2.66	1.09	5.92	5.25
2Ti: 1Zr	28.53	62.23	1.88	2.59	4.77	6.38
1Ti: 2Zr	20.82	73.37	1.99	0.76	3.07	7.57

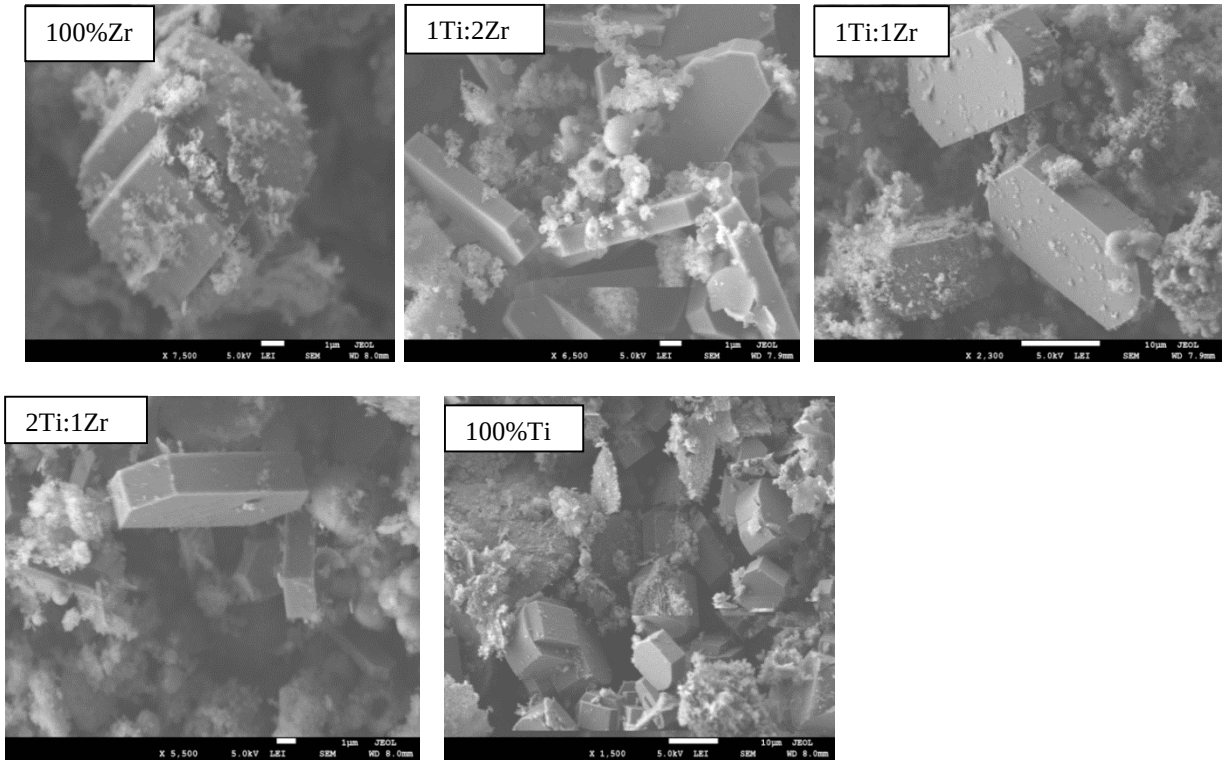

Fig. 4 SEM images of all investigated samples

3.3. Infrared spectra of the samples

Infrared spectra of all Titanium to samples are given in Figure 5. From these figures, it could be observed that there are two regions of peaks one at ~ 550 cm^{-1} which is assigned to the vibrational frequency of framework of ZSM-5 and could be a significant peak for the formation of the ZSM-5 phase. Also, the ratio of I of peak 960-990 to me of the peak at 550 cm^{-1} could be taken as a measure for the incorporation of Ti into the ZSM-5 framework [21].

The other groups of peaks are broad peaks around 800-1300 cm^{-1}. To deeply analyze this region we make a deconvolution analysis for these peaks (Figure 6). From the analysis of this figure, it could be observed that this group of peaks consists of many peaks related to M-O stretching bands where M (Si, Ti, or Zr). Thus as said before the peak at 980 cm^{-1} to the peak of 550 cm^{-1} could be assigned as a relation to the % of Ti incorporated into the framework. It was observed that this peak appears clearly in the pure Ti sample and disappears in the 2Zr:1Ti and pure Zr samples.

Returning to EDX analysis it could be confirmed that the Ti in the orthorhombic crystals is disappeared in these samples indicating that only Zr enters the framework in these samples. Correlation of the intensities ratio of these peaks to data of EDX analysis could give us a good linear correlation (Figure 7). Besides, the other peaks in these regions could be assigned but not accurate to the Zr-O-Si vibrational frequencies.

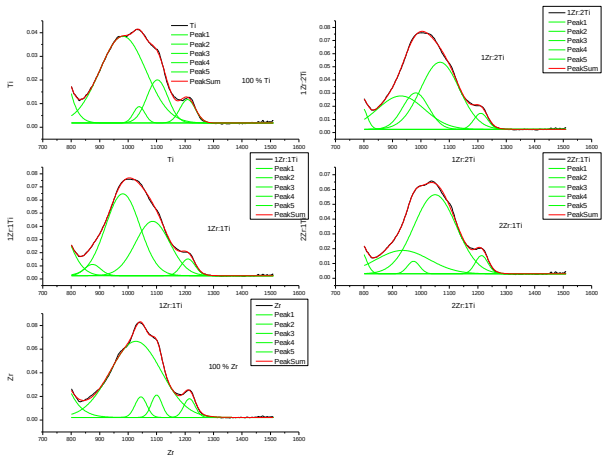

Figure 5 Infrared spectra of all investigated samples

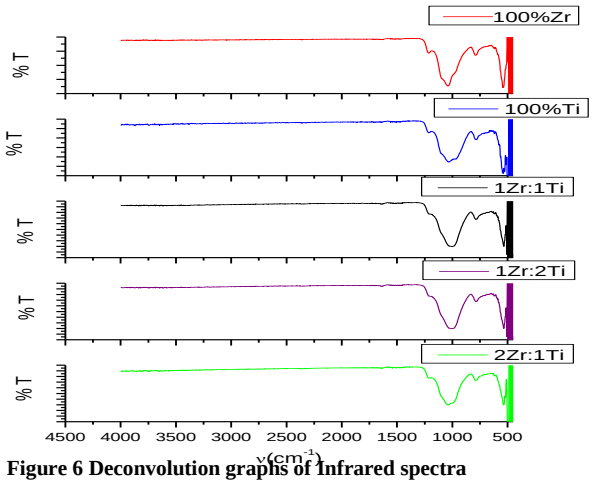

Figure 6 Deconvolution graphs of Infrared spectra

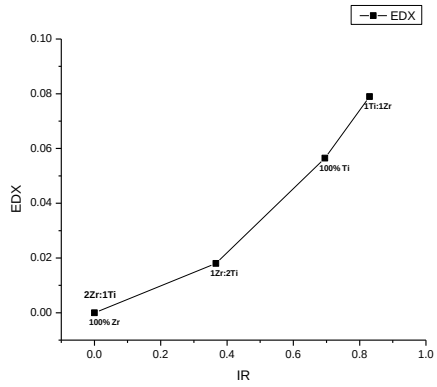

Figure 7 Correlation of Ti/Si from IR (980/550) peaks against real value of elemental analysis of SEM crystal

3.3.1. Diffuse reflectance spectra

The bandgap energy could be calculated from the diffuse reflectance spectra using the Kubelka-Munk method (Figure 8). Details of calculations of this method could be found elsewhere in reference [22]. The bandgap values were found to be about 3.58 eV. This may reflect the crystalline environment of zeolite structure around M^{4+} which puts it in a more restricted environment.

Also, with deep analysis of the diffuse spectra, we can recognize three peaks; one around 220 nm and the other in the center around 255 nm, and the third is around 290 nm. To quantify these peaks, we perform deconvolution analysis using origin 8.5. The results are shown in Figure 9. These results showed that all samples exhibit three peaks with different intensities except that 100% Zr which the peak around 290 nm is missed. Searching the literature for interpretation of these peaks, we found that peak around 220 nm is attributed to tetrahedrally M^{4+} ions [23-24] and peak around 290 is attributed to octahedrally M^{4+} [23, 24] while peak around 255 nm is due to the presence of M^{4+} in the ultra-thin environment and resulting from quantum size effect of nanocrystal [23, 24]. The tetrahedral and octahedral peaks could be quantified and rationalized [24], while, the middle peak around 250 nm could not quantified because of the quantum size effect which may replicate the transition of electrons between the quantum levels.

Thus Table 5 showed the ratio of octahedral and tetrahedral sites in all samples. It is observed that the tetrahedral site is predominate while the existence of octahedral sites gives us any evidence for the formation of some metal silicate rather than ZSM-5 phase with the presence of Ti^{4+} or Zr^{4+} in octahedral positions. Also, the presence of octahedral positions may be reflected in ion-exchange proprieties of ions which will be seen later.

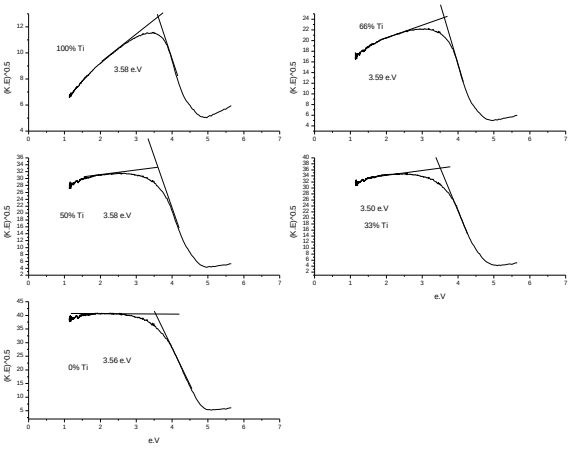

Figure 8 Kubelka-Munk method curves

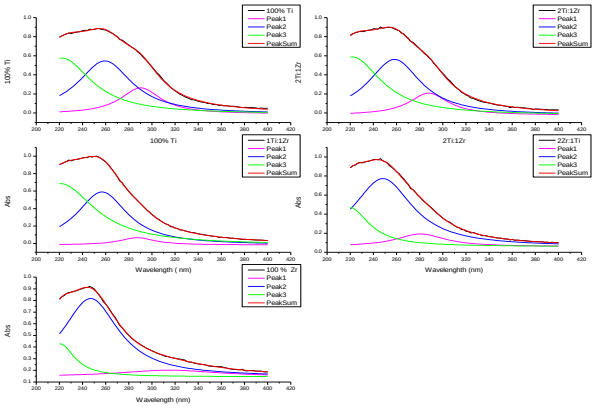

Figure 9 Deconvolution graphs of diffuse reflectance spectra

Table 5 The ratio of octahedral and tetrahedral sites in all samples

	% Tetrahedra	% Octahedral
100% Zr	100%	0
2Zr:1Ti	71.24269	28.75731
1Zr:1Ti	94.45543	5.544566
1Zr:2Ti	79.51581	20.48419
100% Ti	75.82358	24.17642

3.3.2. Simultaneous photodegradation of organic-inorganic pollutants

To achieve this mission we make simultaneous removal of M.B dye with Pb, Cu, Co, and Ni ions with different ratios in the presence and absence of UV Irradiation. To be systematic we first study the effect of different concentrations of dye on the removal of ions and then the effect of ions on the removal of dye.

3.3.2.1. Effect of dye on the removal of ions

To study this effect we make a three-dimensional graph including the total amount of ions removed (Figure 10) against time with different amounts of dye in the presence and absence of UV irradiation. To quantify the effect of dye we select time 60 min and redraw three-dimensional graphs of total ions removed (i.e all amount of ions Pb, Ni, Cd, and Cu) against the composition of zeolites prepared (Figure 11) it is observed from these figures that at 2Zr:1Ti sample an increase in the removal of ions is observed in the presence and absence of UV irradiation. Besides, no observable effect of the concentration of dye on the removal of ions existed. Returning to deconvolution data of diffuse reflectance we can correlate this increase to the number of octahedral sites that exhibit larger values than other compositions. Moreover, irradiation with UV resulted in a slight increase in the removal of ions. This could be regarded as that certain ion is contributing to the photodegradation process which leads us to study the removal of each ion individually (Figures 12-15).

It is observed from these figures that Nickel and Cobalt removal is much more affected by irradiation especially at a lower concentration of dye which may be reflected later when we deal with the mechanism of photodegradation.

3.3.2.2. Effect of amount of ions on the removal of dye

To make this task, variation of the concentration of ions and study its effect on the removal of dye in the presence and absence of UV irradiation was performed. Figures (16-19) represent three-dimensional graphs of different compositions of samples against time and % removal of both ions and dye in the presence and absence of UV irradiation. It is observed that in presence of ions the removal of dye is highly influenced by irradiation. Thus in presence of ions amount of dye removed (adsorbed) is very limited except for sample 2Zr:1Ti which showed high adsorption capability even in presence of ions. However, in all cases a large increase in removal was observed by UV irradiation reflects the photodegradation of the dye. Moreover, no observable effect of irradiation in absence of ions thus the removal of dye is seemed to be due to the effect of only adsorption. In other words, adsorption of dye is observed with the high amount in absence of irradiation hence no observable effect of irradiation hence dye is already adsorbed.

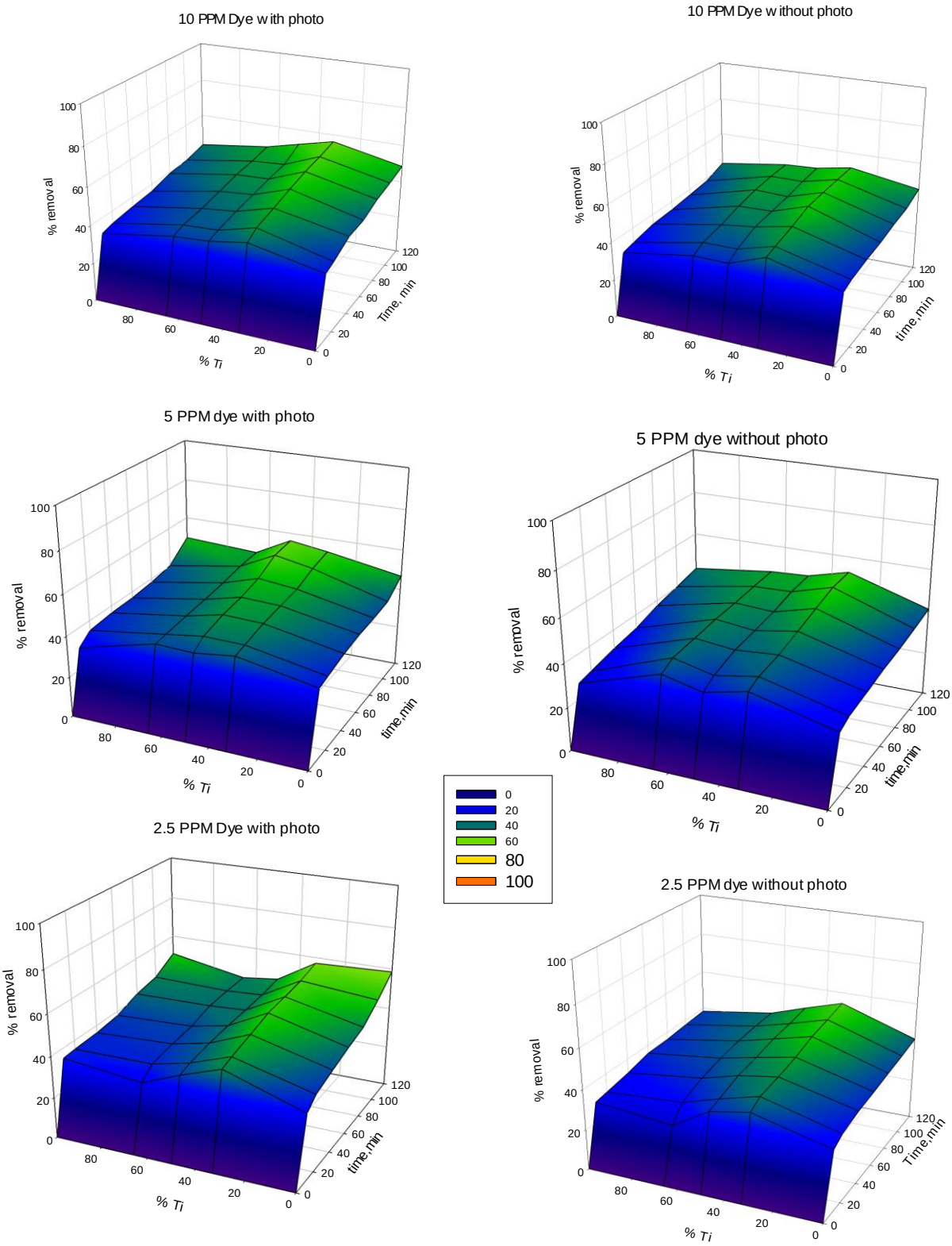

Figure 10 Effect of different concentrations of dye on the total removal of ion.

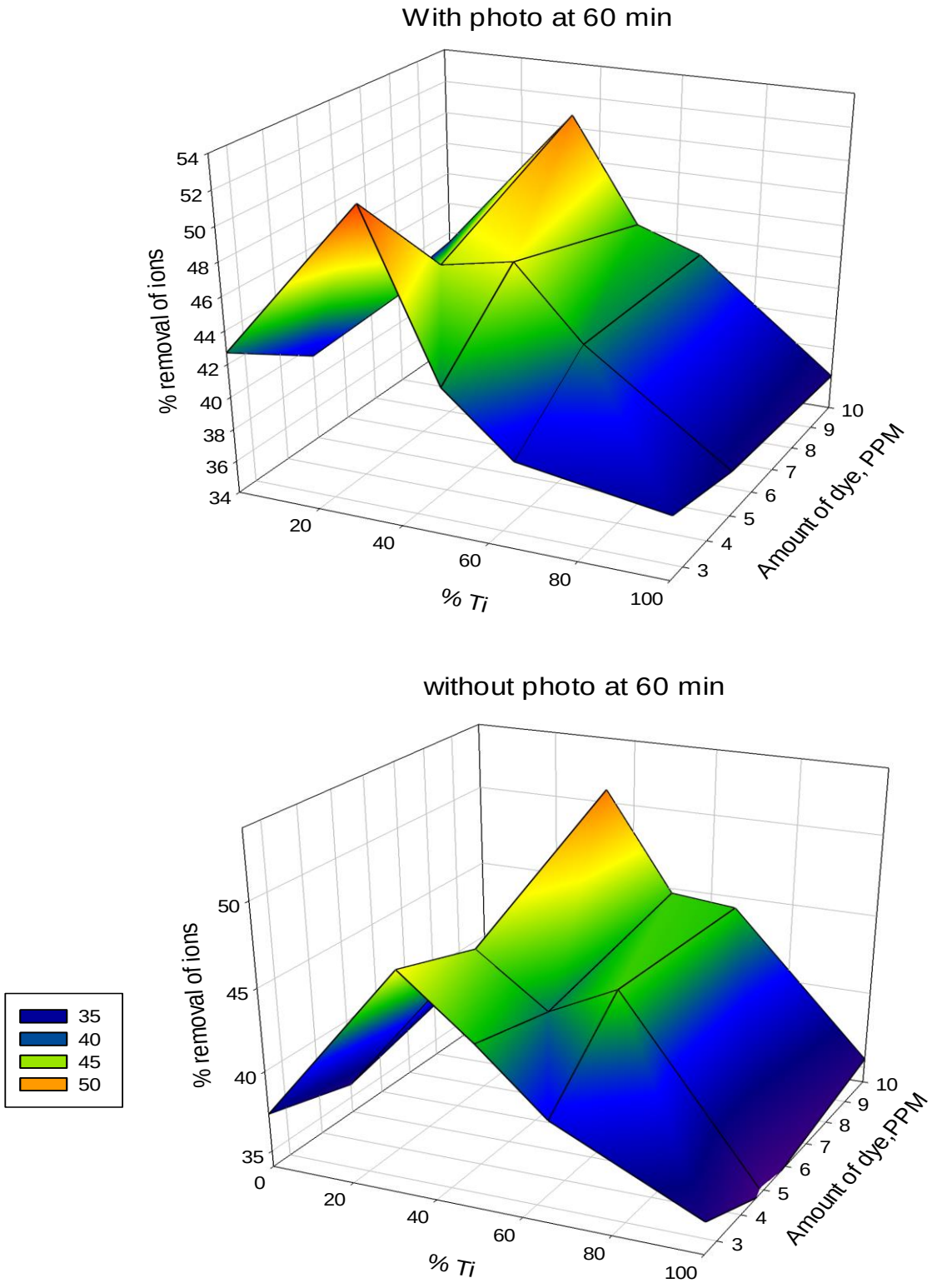

Figure 11 Three dimensional graphs of total ions removed against the composition of zeolites prepared at 60 min.

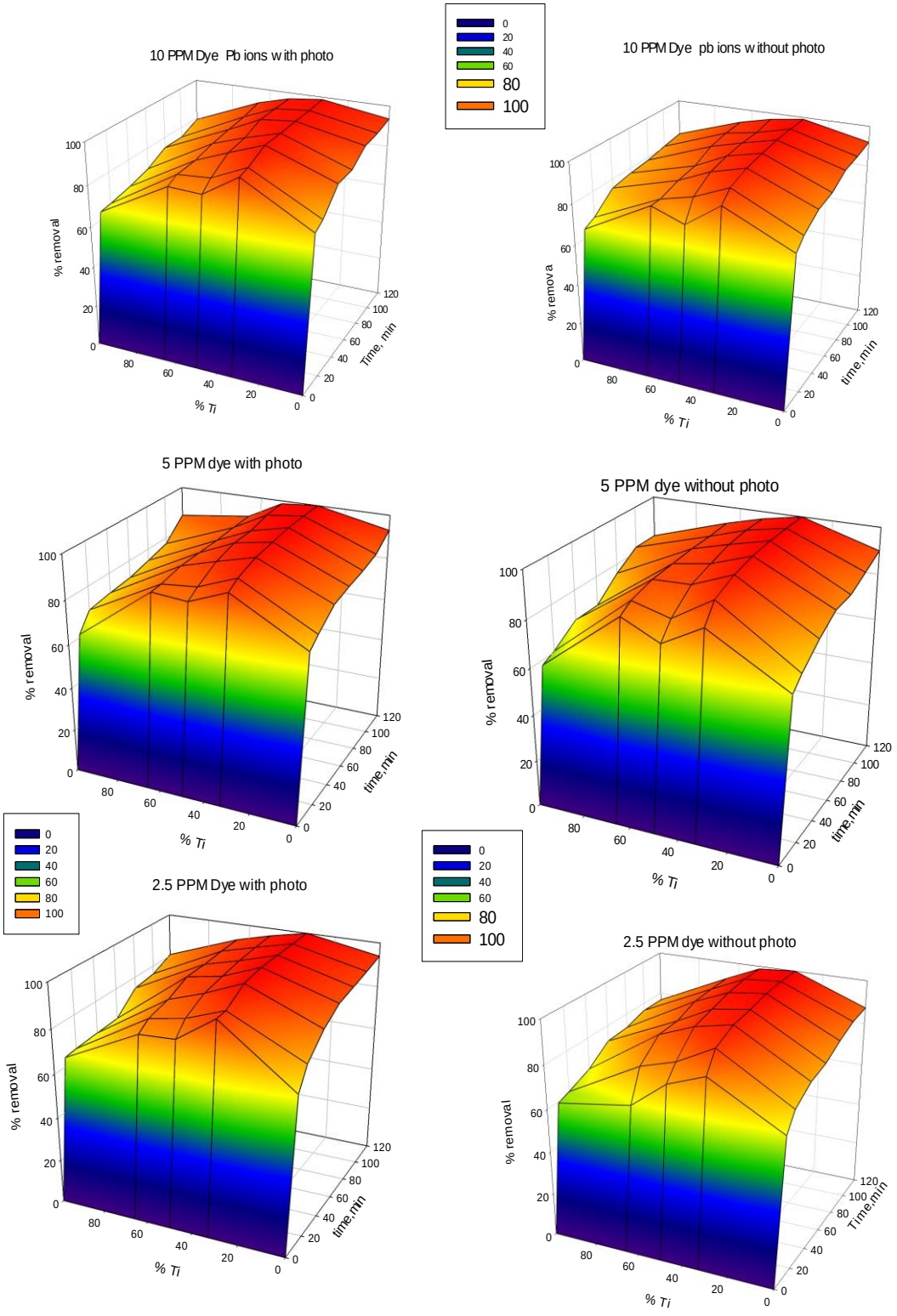

Figure 12 Three dimensional curves of removal of Pb ions with different concentrations of dye in presence and absence of UV irradiation

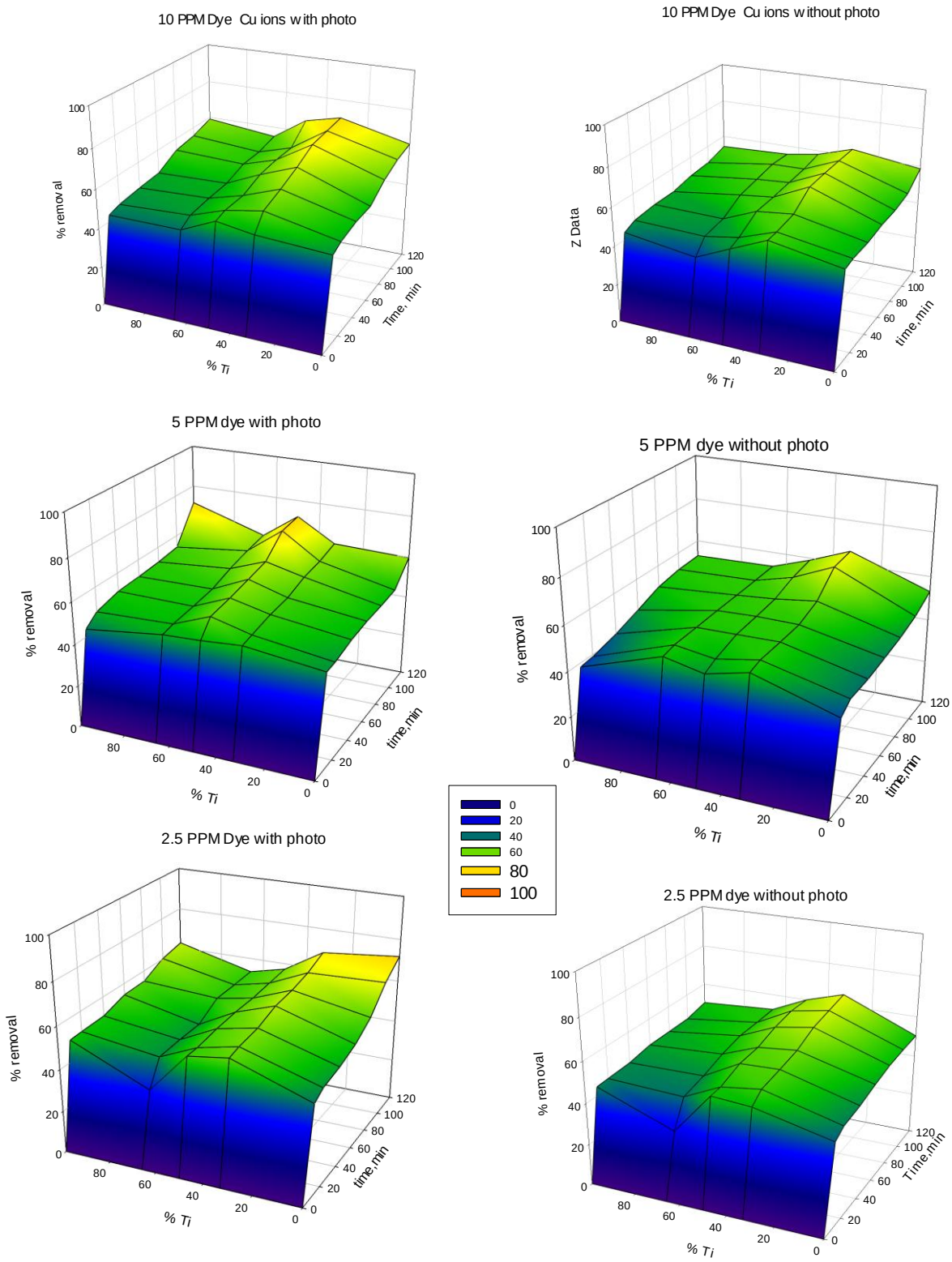

Figure 13 Three dimensional curves of removal of Cu ions with different concentrations of dye in presence and absence of UV irradiation

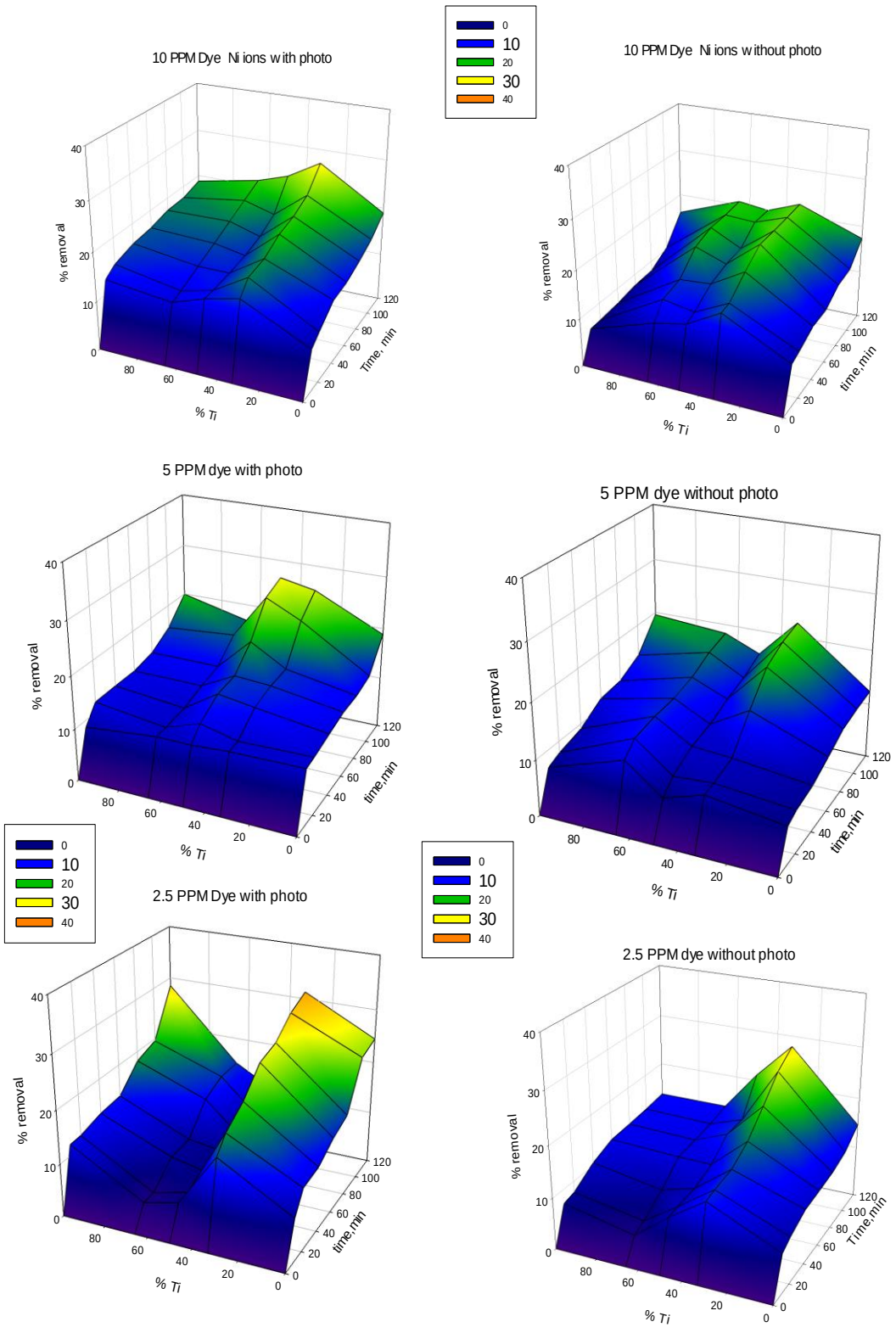

Figure 14 Three dimensional curves of removal of Ni ions with different concentrations of dye in presence and absence of UV irradiation.

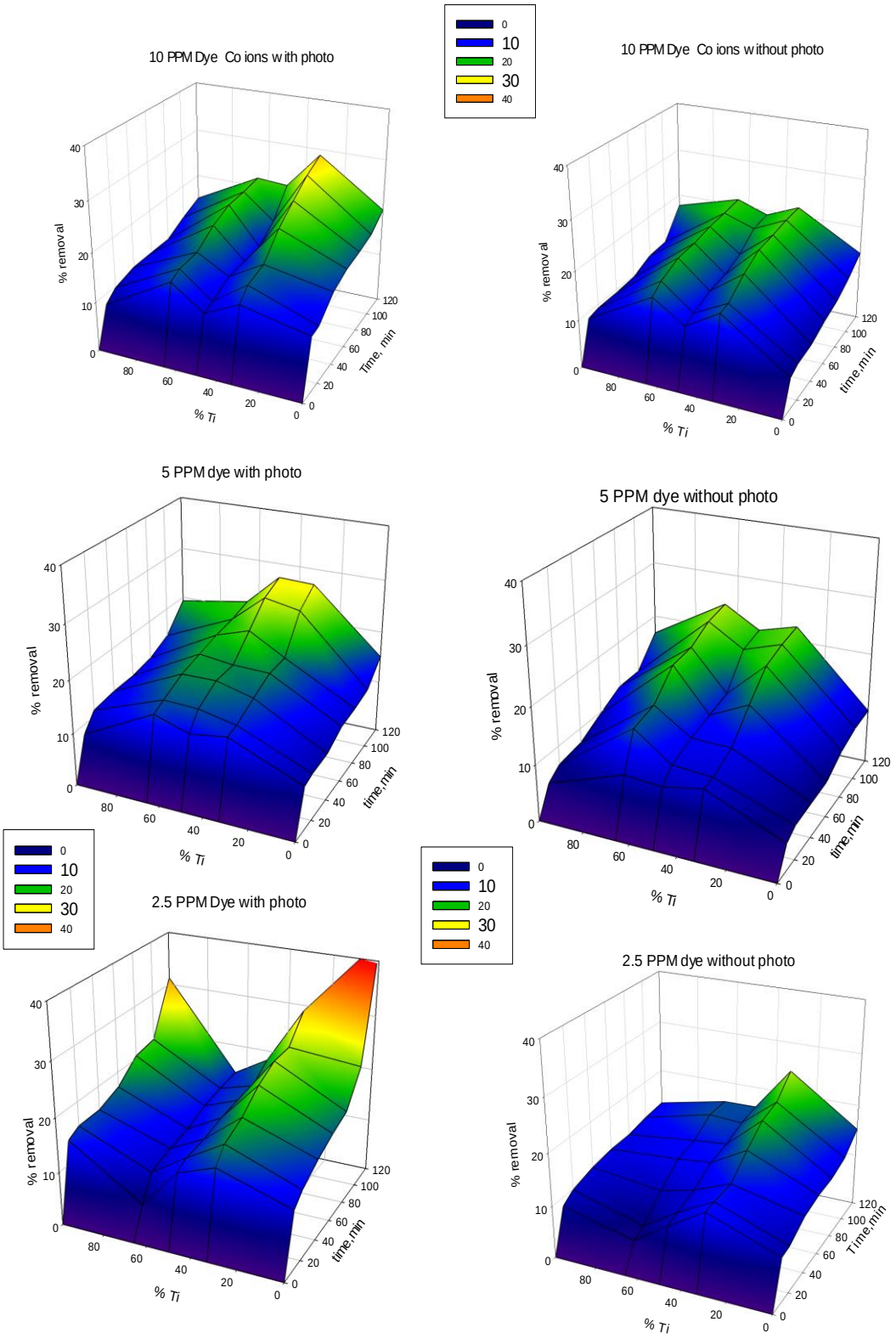

Figure 15 Three dimensional curves of removal of Co ions with different concentrations of dye in presence and absence of UV irradiation

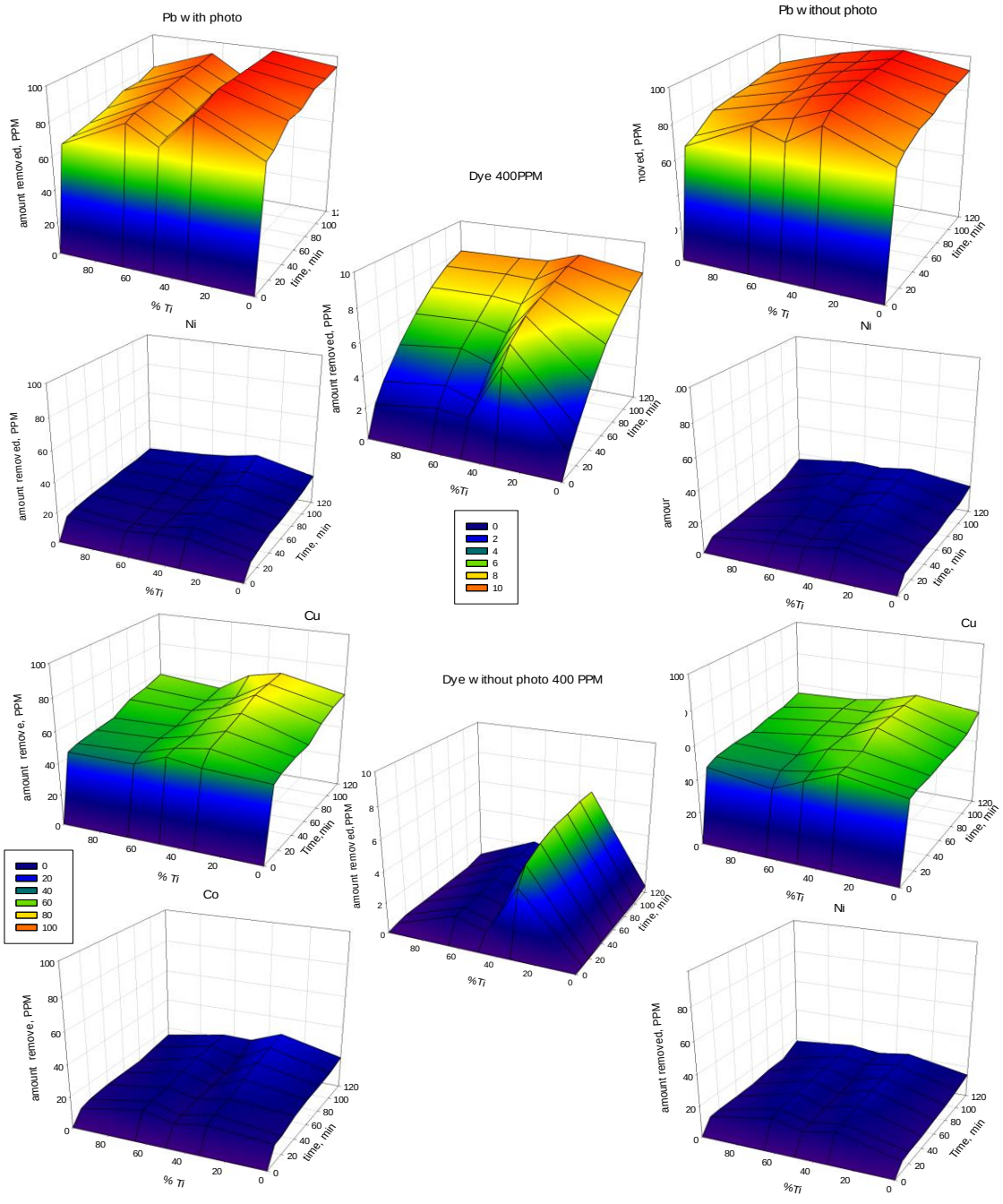

Figure 16 Three dimensional graphs of different compositions of samples against time and % removal of both 400 PPM ions and dye in the presence and absence of UV irradiation.

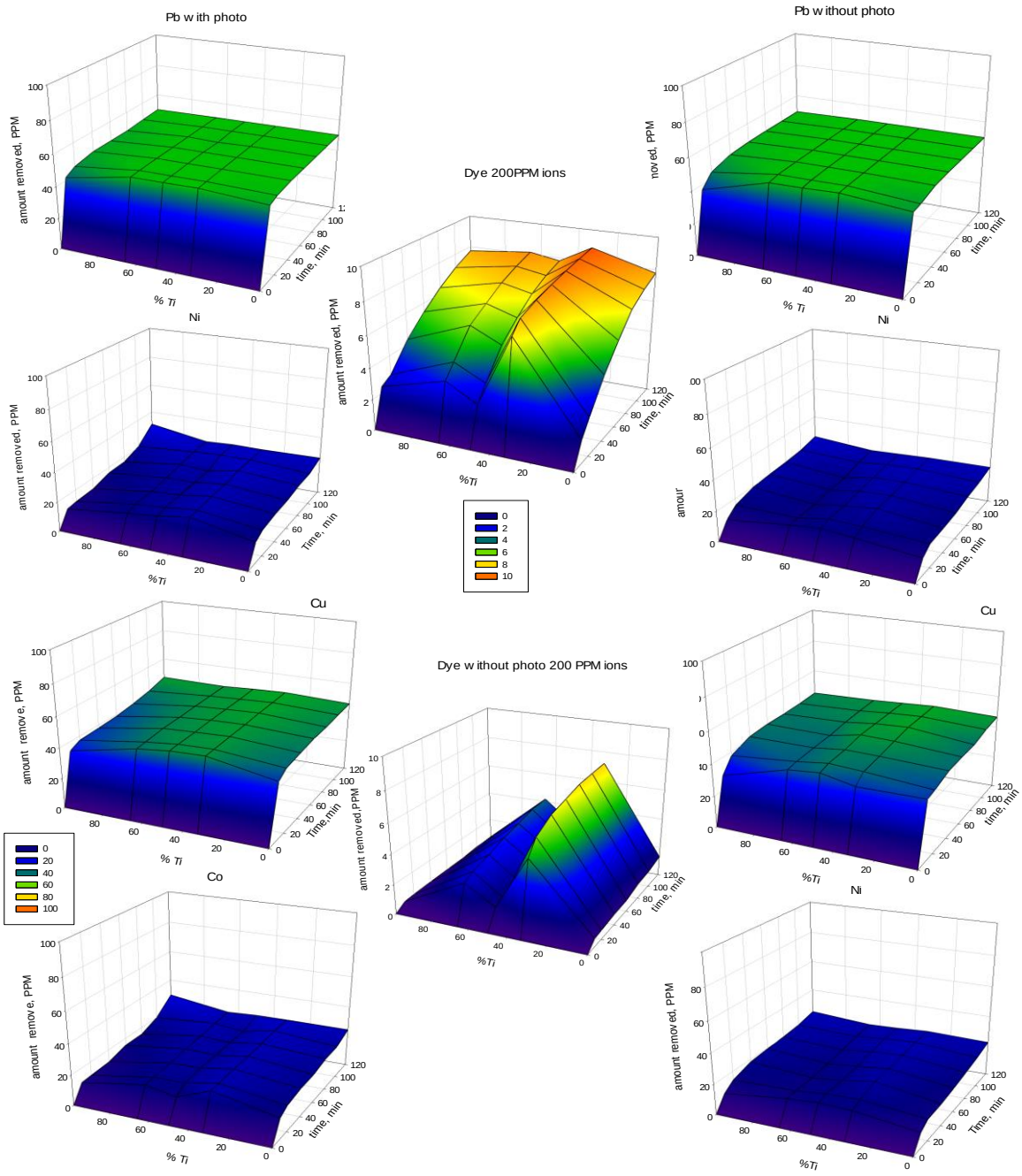

Figure 17 Three dimensional graphs of different compositions of samples against time and % removal of both 200 PPM ions and dye in presence and absence of UV irradiation

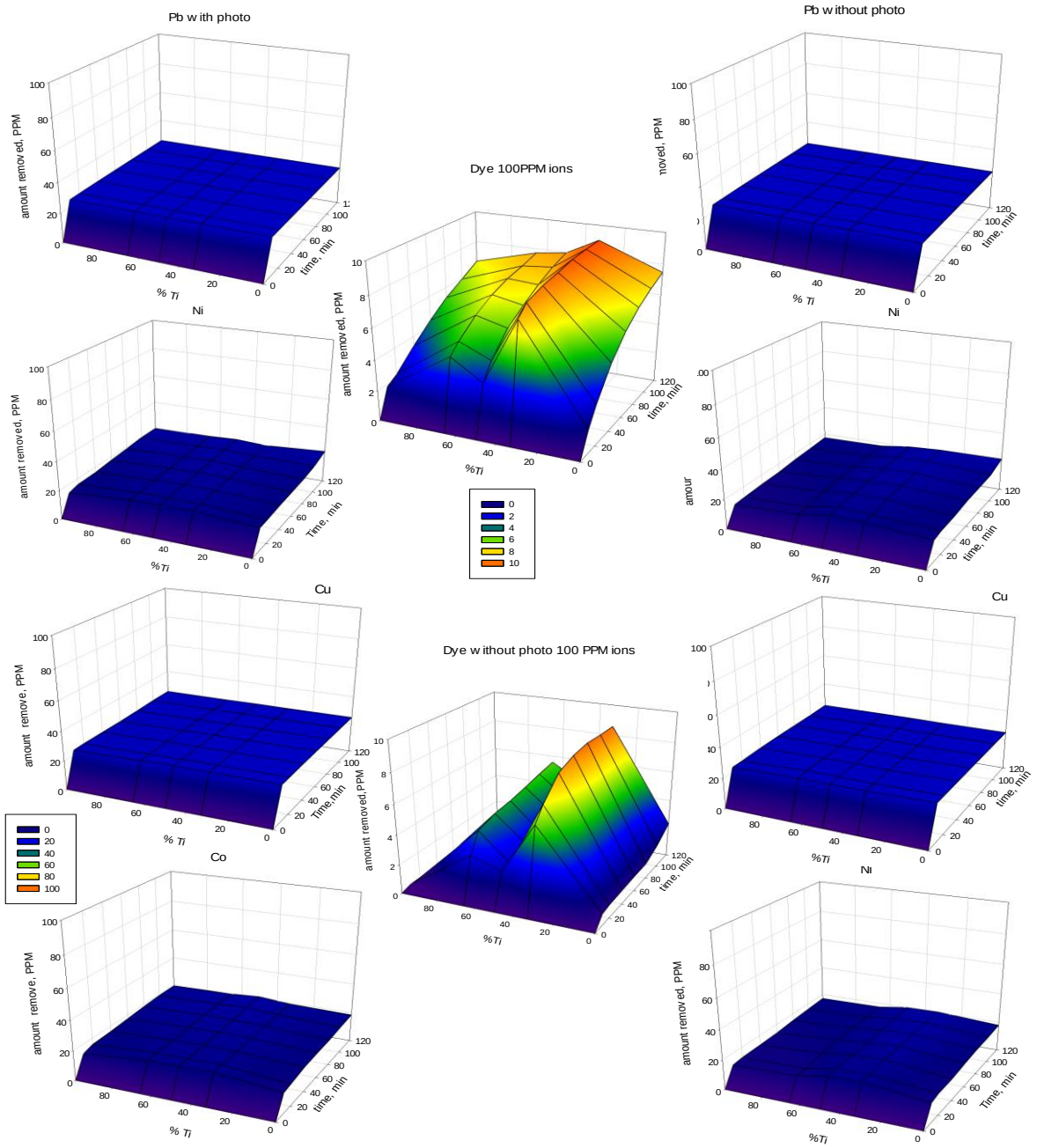

Figure 18 Three dimensional graphs of different compositions of samples against time and % removal of both 100 PPM ions and dye in the presence and absence of UV irradiation.

Figure 20 represents the effect of ions on the removal of dye at 120 min. From this figure, it is observed that the irradiation increases the removal of dye in all concentrations of ions reflecting as we said before the photodegradation behavior.

Figure 21 represents the capacity graph of ions in the presence and absence of UV irradiation at 120 min. from these graphs it clear that the capacity of different samples is nearly affected by neither composition nor irradiation.

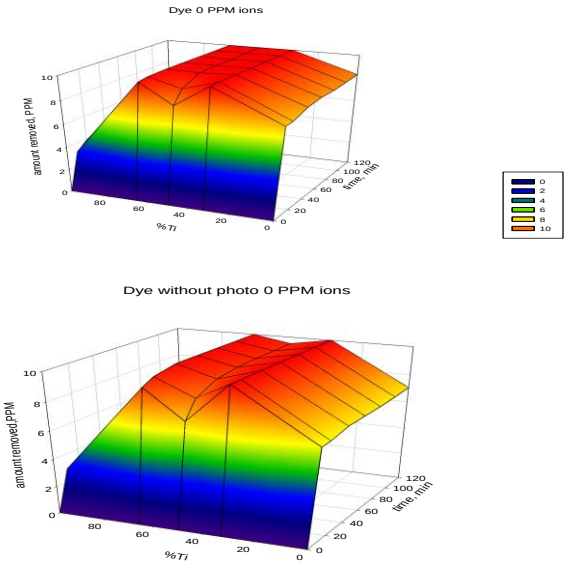

Figure 19 Three dimensional graphs of different compositions of samples against time and % removal of both 0 PPM ions and dye in the presence and absence of UV irradiation.

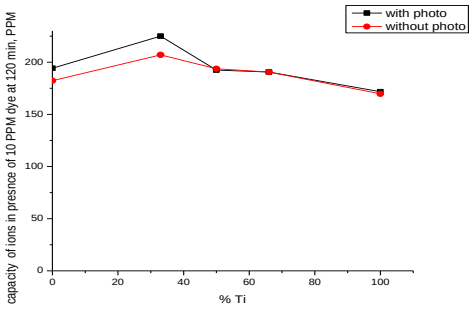

Figure 21 The capacity graph of ions in the presence and absence of UV irradiation at 120 min.

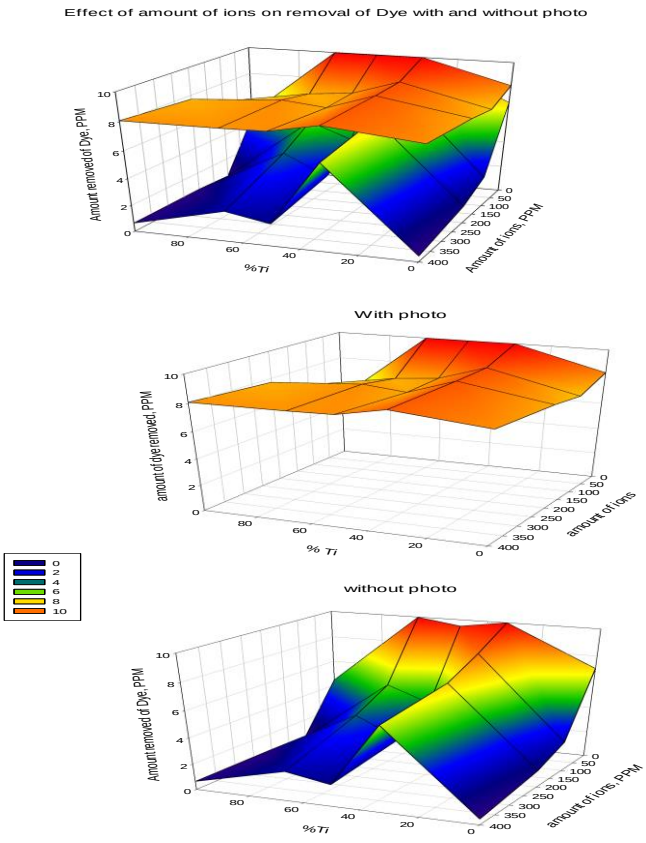

Figure 20 The effect of ions on removal of dye at 120 min

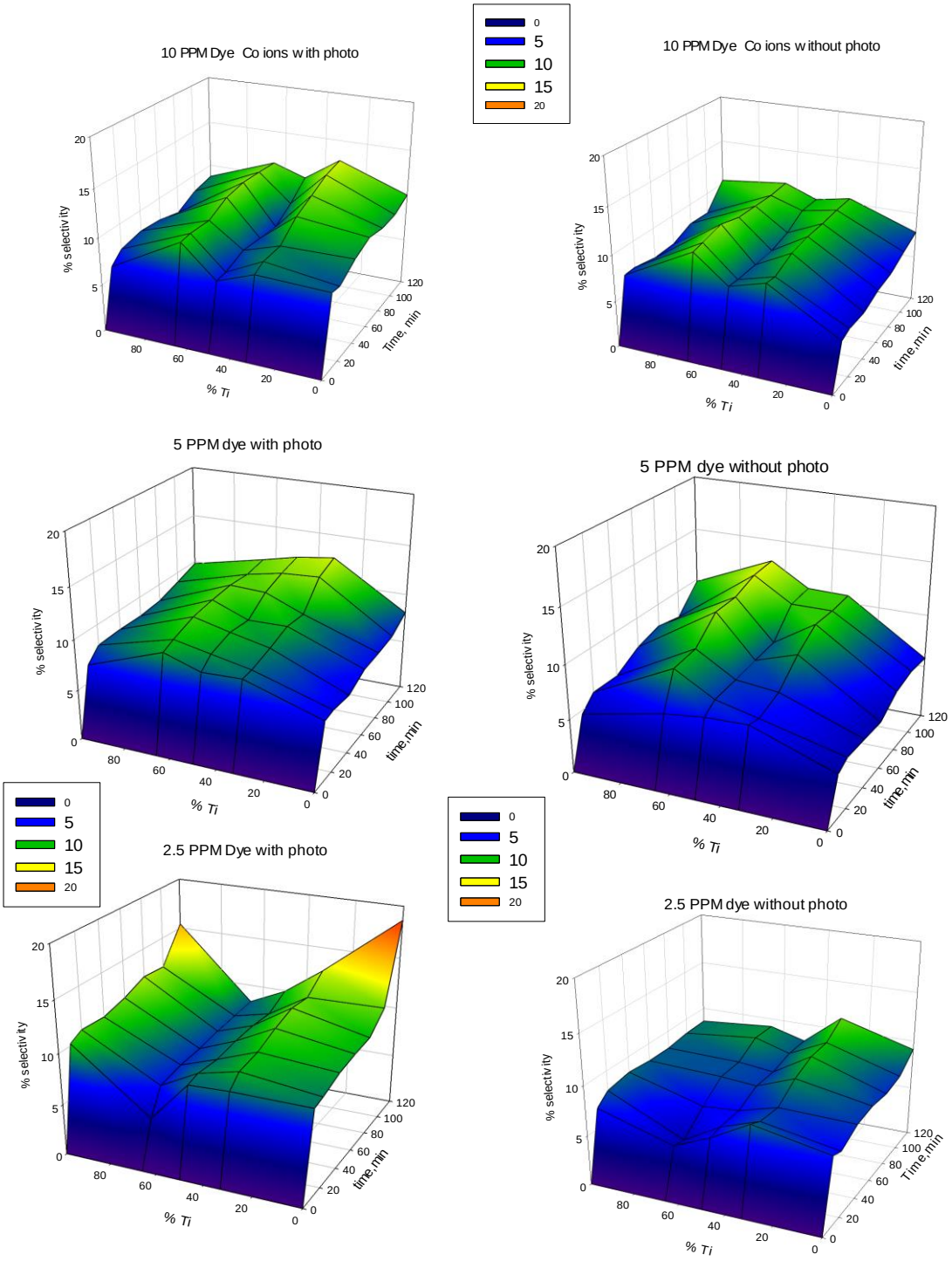

Figure 22 Effect of concentration of dye on the selectivity of cobalt ions.

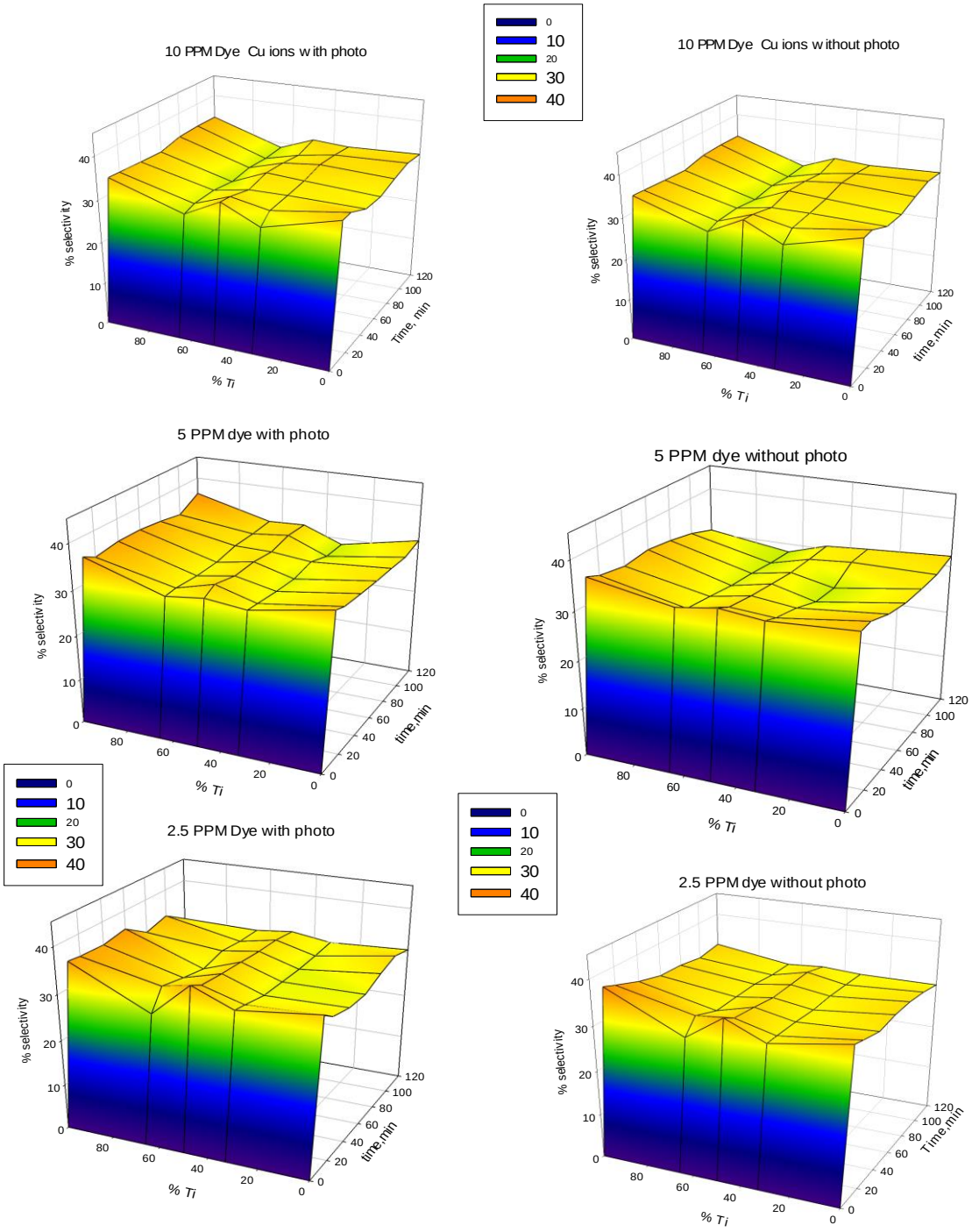

Figure 23 Effect of concentration of dye on the selectivity of copper ions

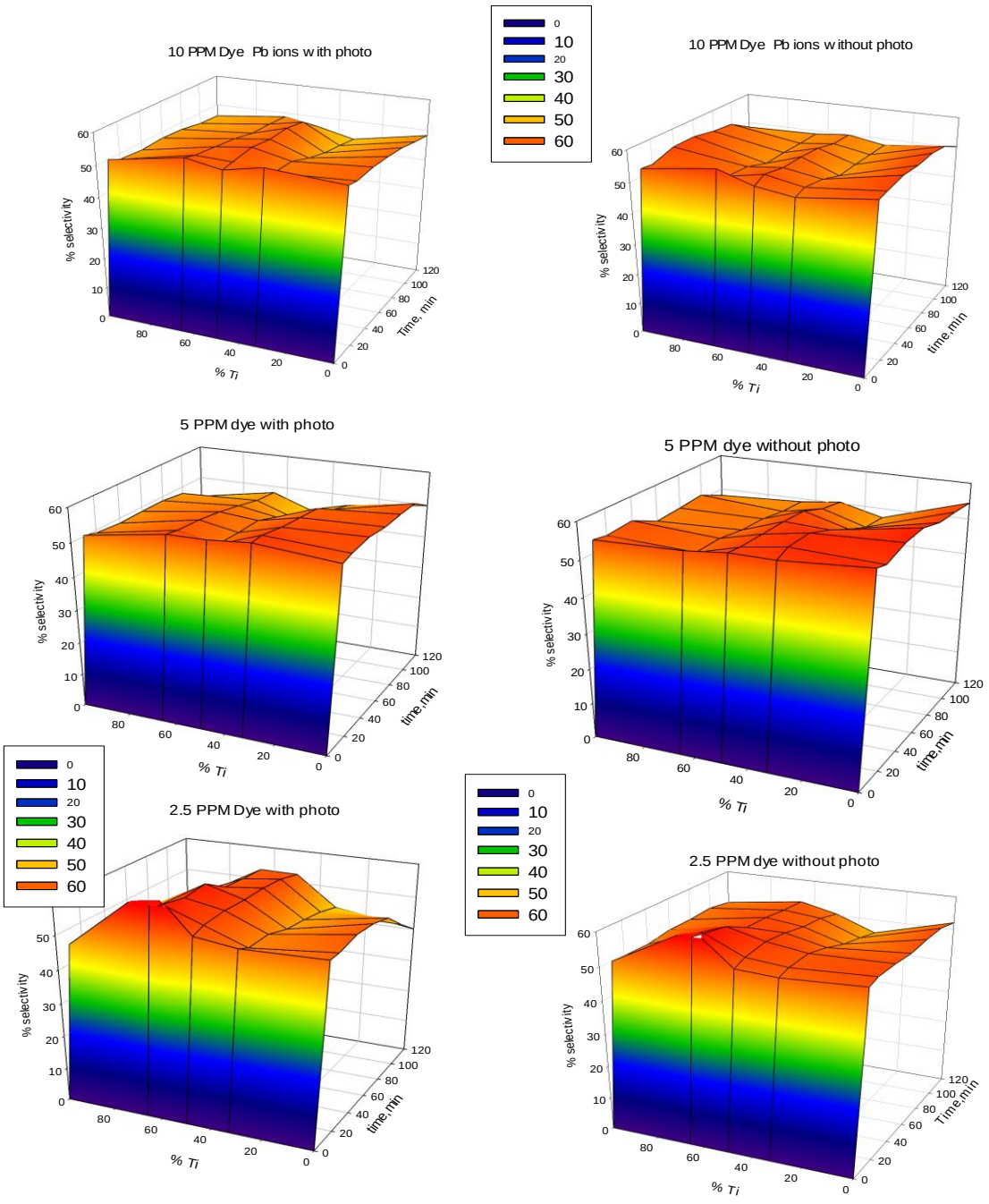

Figure 24 Effect of concentration of dye on the selectivity of lead ions

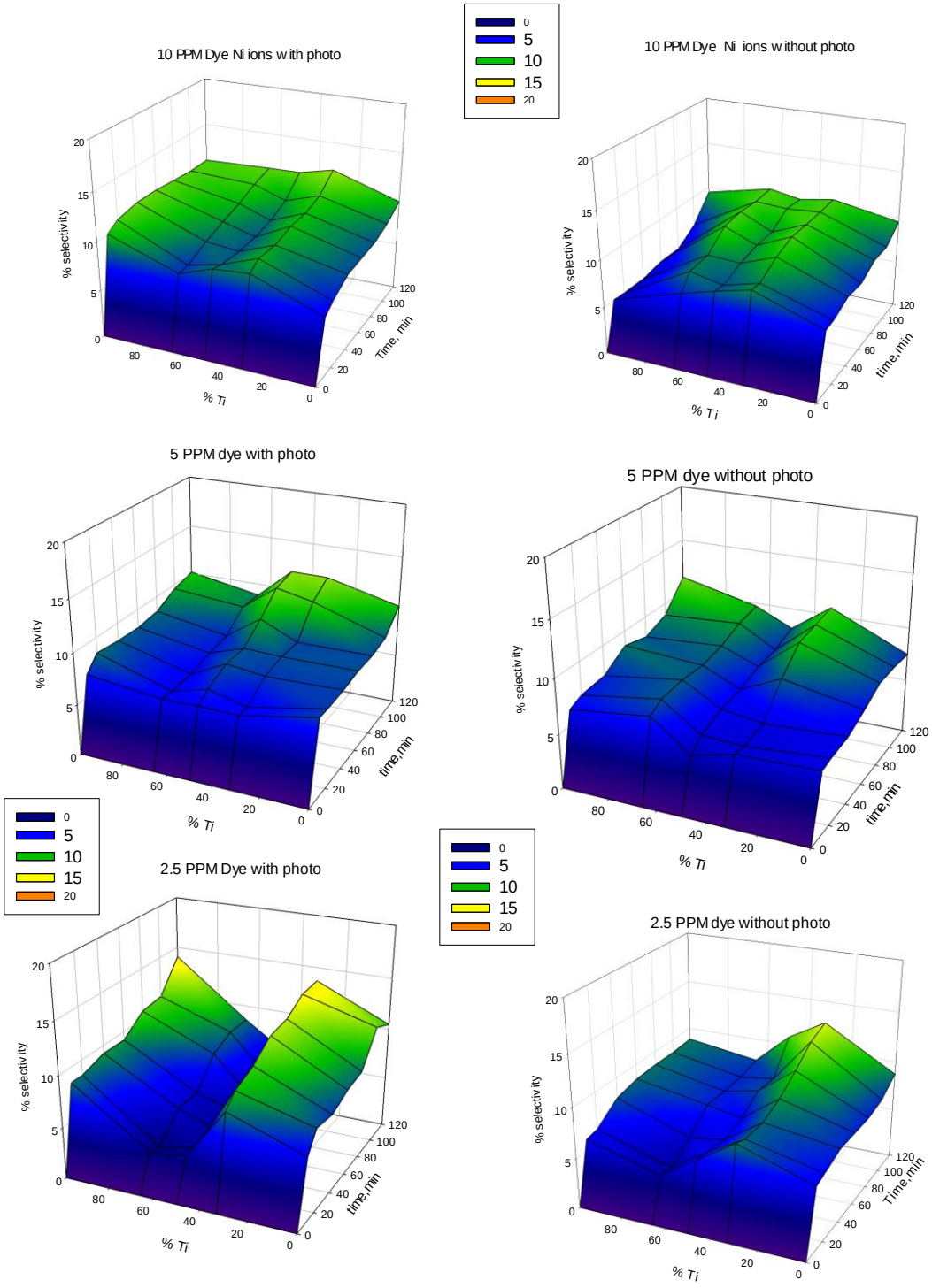

Figure 25 Effect of concentration of dye on the selectivity of Nickel ions.

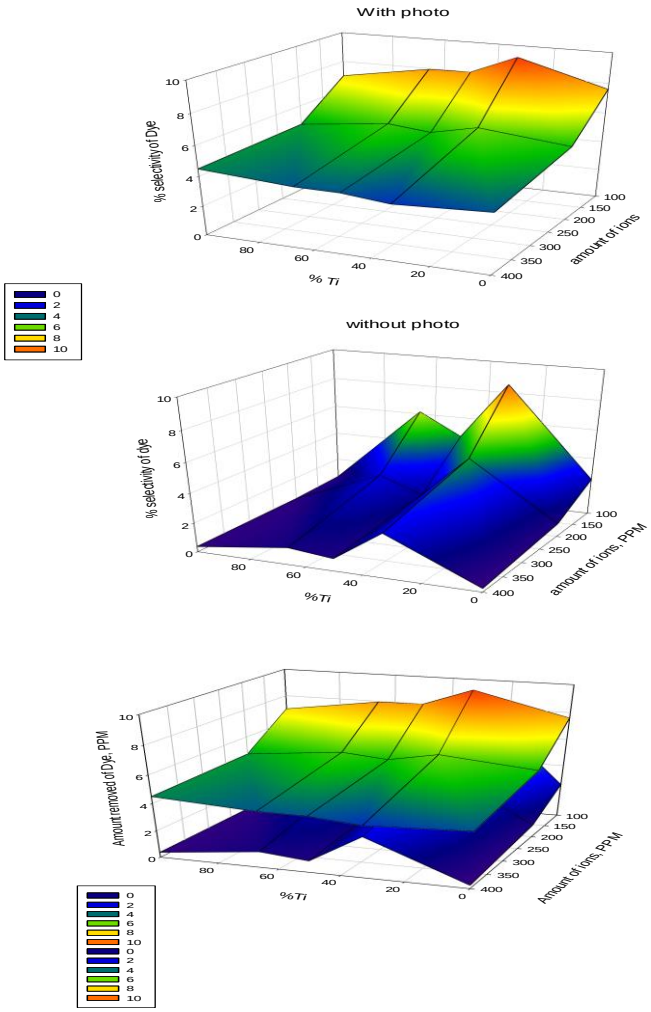

Figure 26 Effect of amount of ions on % selectivity of Dye with and without photo.

3.3.2.3. Effect of selectivity

To deep analyze the effect of ions on photocatalytic degradation we make a graph of selectivity of both ions and dye in the presence and absence of irradiation. From these graphs (Figures 22-26) it could be observed that the selectivity of Pb and Cu is much higher than that of Co and Ni also that the selectivity of dye is increased the effect of irradiation which is reflecting the zeolite composition behavior of ZSM-5 (26). The selectivity of each component is calculated by dividing its amount of removal upon the total amount of removed and/or degraded other components.

3.3.3. Mechanism of photodegradation of Methylene blue

To elucidate the mechanism of photodegradation of MB in presence and absence ions, first, we perform kinetic analysis was performed for pseudo-first and second and third orders, all degradation was found to follow pseudo-first-order. (Table 6)

Table 6 Kinetics summary of samples

	0 ions		100 PPM ions		200 PPM ions		400 PPM ions	
sample	R^2	k	R^2	k	R^2	k	R^2	k
100 % Zr	0.75	0.22	0.87	0.16	0.86	0.16	0.88	0.16
2Zr:1Ti	0.75	0.23	0.76	0.22	0.77	0.22	0.78	0.21
1Ti:1Zr	0.77	0.23	0.80	0.19	0.82	0.18	0.80	0.17
2Ti: 1Zr	0.75	0.23	0.77	0.20	0.79	0.19	0.83	0.18
100% Ti	0.79	0.18	0.80	0.16	0.78	0.17	0.85	0.17

In our case, the Titanium to Zirconium ZSM-5 zeolite matrix is loaded by divalent metal ions. There is more than one evidence that some ions (Co and Ni) are contributing to the photodegradation of M.B dye. The role of ions here could be visualized in the sight that ions attract an electron from the conduction band to be reduced to monovalent state then it reoxidized again leaving this electron to oxygen molecule which transferred to singlet oxygen which is then capable of attacking the dye to degrade (scheme 1).

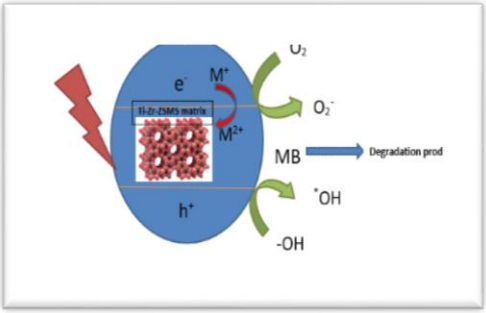

Scheme 1 Mechanism of photodegradation of dye

4. Conclusions

The following conclusions could be drawn from this study:

The incorporated Ti/Zr ZSM-5 structure showed high efficiency for removal of both ions and organic dye

The results showed that Nickel and Cobalt removal is much more affected by irradiation especially at a lower concentration of dye. Deep analysis of DR gives any evidence for the formation of some metal

silicate rather than ZSM-5 phase with the presence of Ti^{4+} or Zr^{4+} in octahedral positions which increases the ion exchange capacity for ions. Also, Ti in the orthorhombic crystals was disappeared. Pb and Cu are much higher than that of Co and Ni in the effect of selectivity.

5. Conflicts of interest

"There are no conflicts to declare".

6. Acknowledgments

This project was funded by the Deanship of Scientific Research (DRS), King Abdul-Aziz University, Jeddah, under grant no. (G: 153-247-1440). The authors, therefore, acknowledge with thanks DRS technical and financial support.

7. References

[1] P. Losch, A. B. Pinar, M. G. Willinger, K. Soukup, S. Chavan, B. Vincent, P. Pale and B. t. Louis, *Journal of Catalysis* **2017**, *345*, 11-23.

[2] X. Mi, Z. Hou, X. Li, H. Liu and X. Guo, *Microporous and Mesoporous Materials* **2020**, *302*, 110255.

[3] H.-h. Wu and G. Li, *Applied Catalysis A: General* **2012**, *423-424*, 108-113.

[4] F. J. Llopis, G. Sastre and A. Corma, *Journal of Catalysis* **2004**, *227*, 227-241.

[5] Z. Shen, C. Ma, J. He, D. Wang, H. Sun, Z. Zhu and W. Yang, *Applied Catalysis A: General* **2019**, *577*, 20-27.

[6] L. G. Tonutti, H. P. Decolatti, C. A. Querini and B. O. Dalla Costa, *Microporous and Mesoporous Materials* **2020**, *305*, 110284.

[7] B. Dou, G. Lv, C. Wang, Q. Hao and K. Hui, *Chemical Engineering Journal* **2015**, *270*, 549-556.

[8] Y. Lu, C. Hu, W. Zhang, Z. Jin, X. Leng, Y. Wang, J. Chen and M. Luo, *Applied Surface Science* **2020**, *521*, 146348.

[9] M. Schwidder, S. Heikens, A. De Toni, S. Geisler, M. Berndt, A. Brí¼ckner and W. Grí¼nert, *Journal of Catalysis* **2008**, *259*, 96-103.

[10] X. Xing, N. Li, J. Cheng, Y. Sun, Z. Zhang, X. Zhang and Z. Hao, *Journal of Environmental Sciences* **2020**, *96*, 55-63.

[11] L.-C. Wang, Y. Zhang, J. Xu, W. Diao, S. Karakalos, B. Liu, X. Song, W. Wu, T. He and D. Ding, *Applied Catalysis B: Environmental* **2019**, *256*, 117816.

[12] C. Wen, C. Wang, L. Chen, X. Zhang, Q. Liu and L. Ma, *Fuel* **2019**, *244*, 492-498.

[13] Y. Cheneviere, F. d. r. Chieux, V. r. Caps and A. Tuel, *Journal of Catalysis* **2010**, *269*, 161-168.

[14] X. Wang, Y. Guo, X. Zhang, Y. Wang, H. Liu, J. Wang, J. Qiu and K. L. Yeung, *Catalysis Today* **2010**, *156*, 288-294.

[15] I. Khan, X. Chu, Y. Liu, S. Khan, L. Bai and L. Jing, *Chinese Journal of Catalysis* **2020**, *41*, 1589-1602.

[16] N. Li, B. Yang, M. Liu, Y. Chen and J. Zhou, *Chinese Journal of Catalysis* **2017**, *38*, 831-843.

[17] L. M. C. Honorio, A. L. M. d. Oliveira, E. C. d. Silva Filho, J. A. Osajima, A. Hakki, D. E. Macphee and I. M. G. d. Santos, *Applied Surface Science* **2020**, *528*, 146991.

[18] U. Kusampally, N. Dhachapally, R. Kola and C. R. Kamatala, *Materials Chemistry and Physics* **2020**, *242*, 122497.

[19] C. V. Reddy, I. Neelakanta Reddy, K. Ravindranadh, K. Raghava Reddy, D. Kim and J. Shim, *Separation and Purification Technology* **2020**, *252*, 117352.

[20] H. Znad, K. Abbas, S. Hena and M. R. Awual, *Journal of Environmental Chemical Engineering* **2018**, *6*, 218-227.

[21] Z. Chen, J. Wang, K. Shen, R. Wang, H. Liu, X. Huang, Z. Tang, Y. Yu and Y. Liu, *Applied Catalysis A: General* **2020**, *591*, 117403.

[22] I. H. A. E. Maksod, A. Al-Shehri, S. Bawaked, M. Mokhtar and K. Narasimharao, *Molecular Catalysis* **2017**, *441*, 140-149.

[23] C.-H. Wu, H. Li, H. H. Fong, V. A. Pozdin, L. A. Estroff and G. G. Malliaras, *Organic Electronics* **2011**, *12*, 1073-1079.

[24] C.-M. Wu, R. Peng, N. M. Dimitrijevic, T. Rajh and R. T. Koodali, *International Journal of Hydrogen Energy* **2014**, *39*, 127-136.